Photonic Materials and Devices

(Invited paper)

N. Peyghambarian

College of Optical Sciences, Material Science and Engineering Department, University of Arizona.

Abstract— Our recent advances in solid-state optoelectronic materials and devices will be reviewed. In the area of glass optics, fabrication of novel microstructured and multicore fibers and their use in realizing single mode lasers will be summarized. In organic and plastic optics, photorefractive polymers for 3D display applications and nonlinear optical polymers for high speed modulators in RF photonic and remote antenna applications will be discussed. Our progress in medical optics including adaptive eyewear and imaging will also be described.

Keywords: adaptive eye wear, glass optics, medical optics, photorefractive polymers, plastic optics,

I. INTRODUCTION

THE research in photonics is multi-disciplinary bringing together various fields of science and technology including physics, chemistry, materials sciences, mathematics, electrical and computer engineering, medical fields and optoelectronics. In this review article, three examples of such research will be described. These examples include fiber optics, plastic and organic optics and medical optics.

II. MICROSTRUCTURE AND MULTICORE COMPACT FIBER LASERS

Compact and robust lasers generating more and more optical power are attractive for numerous uses in industry, defense, or medicine that reach far beyond traditional laser applications. For instance, focused laser beams of the 10-W to 10-kW-classes are used in materials processing such as drilling, cutting, and welding. In addition to the optical power that is required for a specific application there are other key selection criteria including wavelength, reliability, footprint, and energy efficiency. Fiber lasers, a rather new class of truly solid-state lasers, have the potential to leap frog some of their established rivals and compete successfully in various markets.

Fiber lasers have been improved dramatically over the last decade [1]-[11]. They hold great promise because of very high efficiency and exceptional beam quality. Lasing is achieved by stimulated emission from optically excited rare-earth ions such as Nd, Yb, Er, or Tm. Due to the large variety of available rare-earth dopants, fiber lasers can operate at a multitude of wavelengths from the visible to the infrared. High-power fiber lasers and high-coherence fiber lasers have already started to penetrate industrial and sensing markets.

While most fiber lasers have active fiber length that measure in meters, cm-long fiber lasers promise compactness for device integration and single-frequency operation.

Developing short-length fiber lasers presents the major challenges of achieving sufficient pump absorption and providing enough optical amplification. To obtain strong absorption short fiber lasers have generally been core-pumped using rather low-power single-mode laser diodes and the maximum output power of cm-long fiber laser had been limited to the 100-mW level. Recently, first cm-sized fiber lasers with several Watts of optical power have been demonstrated [1]. These lasers were pumped by high-power multi-mode semiconductor laser diodes into the fiber cladding and high doping concentration in special phosphate glass enabled increased pump absorption.

The improving performance of short fiber lasers is directly linked to the development of large core single-mode fibers. The most successful and flexible approach to increase the core size while maintaining single-mode properties present recently developed micro-structured fibers where two-dimensional periodic refractive index structures surround the fiber core [2]. Applying a special micro-structured fiber design[3] in combination with highly doped phosphate glass 4.7-W output has been demonstrated from a fiber laser with only 3.5-cm of active single-mode fiber corresponding to a yield above 1.3-W per cm (see Fig. 1). An slope efficiency of ~20% with respect to the launched pump. The output spectrum is centered at 1535 nm with a linewidth of ~2 nm.
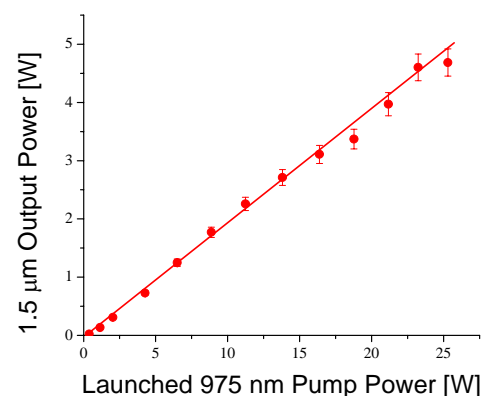

Fig. 1 Signal vs. launched pump power of a 3.5-cm phosphate PC fiber laser.

It has also been shown that a single-frequency linear-cavity fiber lasers can be build when a narrow band fiber Bragg grating (FBG) is utilized as part of the short laser cavity. Using 3.8-cm of active fiber and a laser design as shown in Fig. 2 more than 2-Watt single-frequency output has been obtained.

The flexibility of micro-structured fiber fabrication en-

ables another approach to improve fiber laser perform-ances. Incorporating several active cores into the same cladding, as shown in Fig. 3, the active volume per fiber length can be multiplied promising a further increase in output power per unit length. Fig. 4 shows that more than 15 W of 1.5 μm signal power can be generated from a 10 cm long fiber that contains 19 active cores. These cores are simultaneously pumped through their common cladding and it has been demonstrated that their emission can be coherently combined into one laser beam [11].
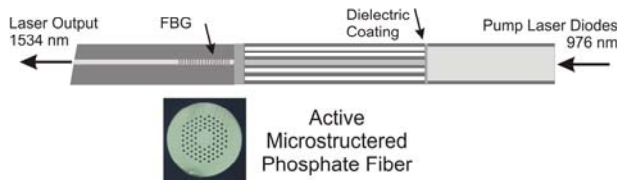

Fig. 2 Design of a cladding pumped single-frequency fiber laser using micro-structured large core active phosphate fiber.

Microstructured optical fibers are certainly amongst the most active research areas in fiber technology and a lot of challenges remain before the full potential can be ex-ploited. Their design flexibility and multiple promising applications fostered rapid progress in fabrication tech-nologies. Besides the demonstrated benefits for cm-sized Watt-level light sources, micro-structured fibers will facili-tate improvements in kW-level fiber lasers and pulsed fi-ber lasers and amplifiers with high peak powers.
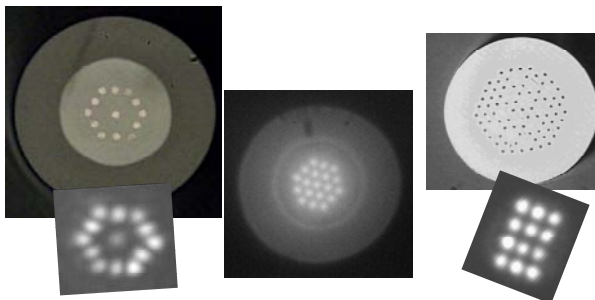

Fig. 3 Multi-core phosphate fibers and their emission patterns.

III. . ORGANIC PHOTONICS

Organic and polymeric optoelectronic materials and de-vices have made tremendous progress over the last ten years, making the journey from laboratory curiosity to emerging commercial products in a number of important areas such as displays, optical communications, solar cells, and data storage. Organic light emitting diode (OLED) technology has already achieved significant penetration in the commercial marketplace for small, cheap and flexible displays. The flexibility of organic chemistry coupled with the knowledge of the device requirements can be used to design molecules and polymers for new applications. Our program in organic optoelectronics encompasses areas such as electro-optic polymer modulators, organic light emitting diodes, photorefractive polymers, sol-gel nano-composites, and infiltrated photonic crystals. The emphasis is on exploiting relatively well-developed materials tech-nologies in novel device geometries that enhance perform-ance, as well as the demonstration of low-cost fabrication

techniques that can lead to high-volume manufacture. New materials are inserted within proven device and fabrication platforms to provide for direct comparison with existing systems. In this article, two recent examples will be high-lighted that show the development of organic optoelec-tronic materials for key existing and emerging photonics applications.

A. Dynamic Holography with Photorefractive Polymers

Photo-refractivity was first observed in doped perovskite electro-optic crystals such as lithium niobate [12]-[24]. The photorefractive effect refers to the genera-tion of an index change associated with the combination of a spatial distribution of charges and the electro-optic ef-fect. In general, it is possible to write dynamic gratings in photorefractive materials that can perform functions such as optical phase conjugation, optical beam clean up, real-time image processing, and two-beam coupling.
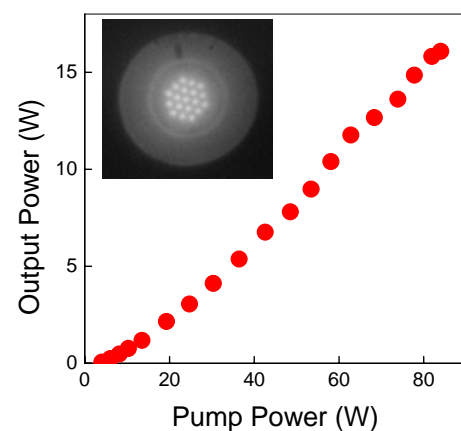

Fig. 4 Signal vs. pump power of a 10 cm phosphate multicore fi-ber laser.

With emergence of electro-optic polymer materials in the late 1980s, it was realized that polymeric photorefrac-tive materials could be made, and the first demonstrations occurred in the early 1990s. These initial proof-of-principle demonstrations established the basic rules by which polymeric photorefractive materials are still made today. The key components of photorefractive polymers are a hole-transport polymer matrix, a sensitizing dye for absorption of the incident radiation, an electro-optic chro-mophore, and, often, a plasticizing material that lowers the T_g of the hole transport matrix. Low T_g is desired, since the electro-optic effect is actually achieved by application of an electric field that serves to orient the electro-optic chromophores. In some cases one molecule can serve sev-eral of these functions, but it has been found, as is the case in xerography and lithographic materials, that composites based on molecules which each provide a unique function-ality have the best combination of performance, reliability and cost.

This general paradigm has been applied with spectacular results over the last ten years, whereby now photorefrac-tive polymers compete with and in many ways outshine their inorganic counterparts. Fig. 5 illustrates the compo-nents of a state-of-the-art photorefractive polymer devel-oped by the University of Arizona and Nitto Denko Tech-nologies. The hole transport matrix, PATPD, has a poly-

acrylic backbone coupled to the well-known hole-transport materials tetra-phenyl-diamino-bi-phenyl (TPD), and provides high hole mobility and other excellent properties. The electro-optic chromophore is 4-homopiperidino ben-zyl-idine-malo-nitrile (7-DCST), the plasticizer is ethyl carbazole (ECZ) and the long-wavelength sensitizing dye is 2-[2-{5-[4-(di-*n*-butylamino)phenyl]-2,4-pentadienylidene}-1,1-dioxido-1-benzothien-3(2*H*)-ylidene] malono-nitrile (DBM). The samples shown in Fig. 5 are 105 μm thick films of this composite sandwiched between ITO coated glass slides, and the fabrication is performed using a melt process.
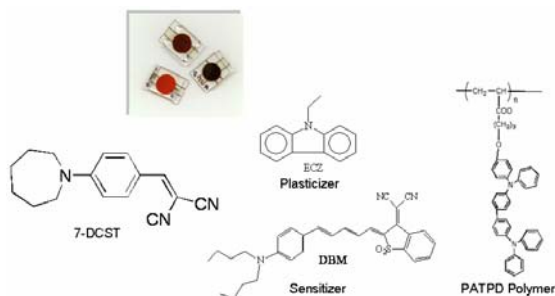

Fig. 5 Components of state-of-the-art polymer photorefractive composite and some typical samples.

To characterize the PR properties written in the samples, four-wave mixing experiments were performed in standard tilted-sample geometry. Two interfering s-polarized beams of equal fluencies (0.5 W/cm^2 each) were used to write the grating and a weak counter-propagating p-polarized beam was used to probe the efficiency of grating. The writing beams were incident on the sample at an inter-beam angle of 20^0 in the air and the sample surface was tilted 60^0 relative to the writing beam bisector resulting in a grating period of 3.1 μm. Fig 6 shows the diffraction efficiency reaches 80% at a field of near 1 KV for a 20μm thick device. It should be noted that the field is only the poling field and does not generate any current.

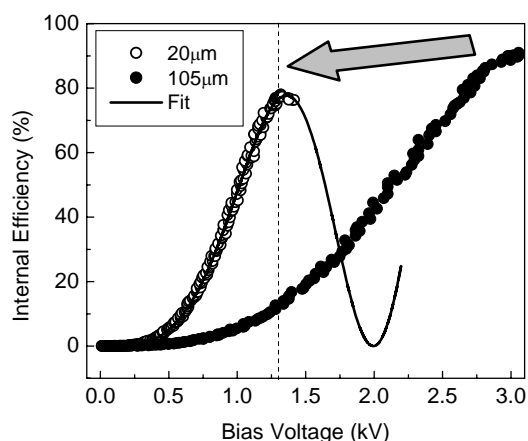**Fig. 6** Steady-state diffraction efficiency for both 20μm and 105μm thick devices, as the bias voltage is increased. When the device thickness is reduced by 5 times, the operating voltage has dropped by a factor of 2.3. The peak internal efficiency was 80%. External efficiency was around 58%, which is higher than a similar thick device, due to low absorption of thin device. The index modulation was 0.0025 at 1.3kV.

In summary, significant research progress has been made and commercialization of photorefractive polymers is already underway. The wide spread commercialization process will be enhanced with improvements in critical areas such as the phase stability of the composite materials, the achievement of sub-millisecond response times, and the reduction of the required applied poling fields to the 10 V/μm level.

B. Nonlinear Electro-Optic Polymers and Devices

For high speed electro-optic (EO) modulation, the standard material has long been lithium niobate, by virtue of its relatively large electro-optic coefficient $(r_{33} = 30\ pm/V)$, good waveguide technology, and relatively good stability [25]-[30]. However, since lithium niobate's electro-optic effect derives primarily from the motion of nuclei in the crystal's lattice, at high modulation rates the efficiency of the response begins to diminish. At the same time, the large mismatch between the refractive index and the square root of the dielectric constant leads to a velocity mismatch for traveling wave modulators, leading to complex, narrow bandwidth designs. In contrast, EO polymers derive their EO effect entirely from electronic motion and have virtually no velocity mismatch, making them ideal for high speed devices; indeed EO polymer modulators operating at greater than 100 GHz have been demonstrated. Progress in the design of the organic dye molecules that give EO polymers their EO coefficient has led to the demonstration of materials with $r_{33} = 370\ pm/V$ at telecommunications wavelengths, providing the capability to make modulators with low operating voltages.
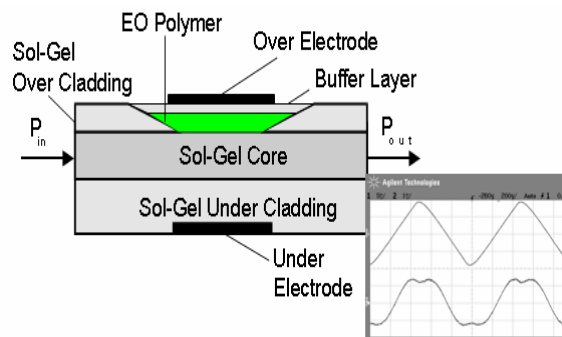

Fig. 7 Hybrid sol-gel/EO polymer modulator showing modulation achieved.

However, EO polymers are still challenged by several important issues including high fiber-to-waveguide coupling loss, high propagation loss, relatively poor thermal stability, and low optical damage thresholds. The latter is directly related to the photo-oxidative stability of the dye molecule, while the thermal stability is related to the freedom of motion of the dye molecule in the host polymer matrix. The dye molecule or chromophore must be oriented in the host polymer by raising the polymer to a temperature near its T_g and then applying a relatively strong electric field (50 – 100 V/μm) to the polymer. The film is then cooled down with the field still applied, which results in many of the chromophores being locked in place, but over time they will deorient through natural statistical fluctuations in the polymer. To impede this deorientation, the chromophore needs to be covalently bound to the polymer matrix, which can occur prior to fabrication, or through a

cross-linking process during fabrication.

High propagation loss and high fiber-to-waveguide coupling losses are more fundamental issues that to date have been difficult to address. One approach to this problem is to use the schematic device shown in Fig. 7. In this case the fiber input and output areas of the waveguide modulator consist of passive MAPTMS-based sol-gel waveguides; this provides for the ability to match the waveguide mode very well to standard optical fiber. The UV-patterning capabilities of the sol-gels are then used to create an adiabatic vertical taper that gradually moves the waveguide mode up into an electro-optic polymer layer, and then back down into the passive sol-gel waveguide at the exit to the device. A low index buffer layer is finally deposited on the EO polymer layer to provide optical confinement and isolation from the top electrode. These devices have demonstrated low insertion losses and the best operating voltage, V_π of 1 Volt. Fig. 7 further shows the optical modulation achieved, as measured through crossed polarizers

IV. PHOTONICS FOR VISION CORRECTION

Presbyopia is an age-related loss of accommodation of the human eye that manifests itself as inability to shift focus from distant to near objects [31]-[34]. Assuming no refractive error, presbyopes have clear vision of distant objects; they require reading glasses for viewing near objects. Area-divided bifocal lenses are one example of a treatment for this problem. However, the field of view is limited in such eyeglasses, requiring user to gaze down to accomplish near vision tasks and in some cases causing dizziness and discomfort. We have investigated a new switchable, flat, liquid crystal diffractive lenses that can adaptively change their focusing power. The operation of these spectacle lenses is based on electrical control of the refractive index of a 5 μm-thick layer of nematic liquid crystal using a circular array of photolithographically defined transparent electrodes. It operates with high transmission, low voltage (< 2 V_{RMS}), fast response (< 1 second), diffraction efficiency exceeding 90%, small aberrations, and a power-failure-safe configuration. These results represent significant advance in the state-of-the-art in liquid crystal diffractive lenses for vision care and other applications. They have the potential of revolutionizing the field of presbyopia correction when it is combined with automatic adjustable focusing power.

We employ a photolithographically patterned thin diffractive lens with large aperture, fast response time, and a power-failure-safe configuration. Fig. 8 (a) compares the shape (phase profile) of a refractive lens (dashed line) with an ideal diffractive lens (dotted line). The diffractive lens is produced by removing the multiple 2π-phase retardation from the refractive lens, resulting in multiple Fresnel zones. The phase jump at each zone boundary is 2π for the design wavelength. To digitize the process, the continuous phase profile in each zone is divided into multiple sub-zones with a series of discrete phase levels ("staircase" structure, Fig. 8a). Diffraction efficiency increases by increasing the number of sub-zones reaching maximum values of 40.5%, 81.1% and 95.0% for lenses with 2, 4, and 8
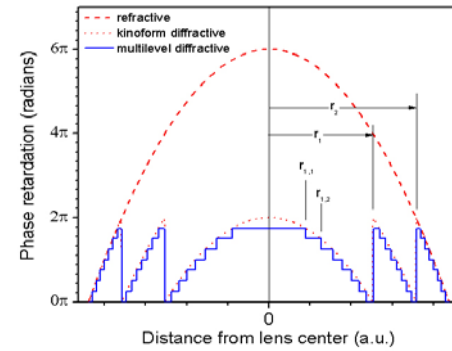
phase levels per zone, respectively.

Fig. 8 Dashed line shows the phase profile of a conventional refractive lens; Dotted line, phase profile to achieve a diffractive lens; Staircase structure, multi-level quantization approximates the continuous quadratic blaze profile.

Diffractive lenses with eight sub-zones, 10 mm diameters and focal lengths of 1 m and 0.5 m (+1.0 diopter and +2 diopter of add power, respectively) were demonstrated at the peak of the human photopic response, 555 nm. Using photolithographic techniques, concentric and rotationally symmetric transparent indium tin oxide (ITO) electrodes (50 nm in thickness) were patterned on a float-glass substrate. A 1 μm gap was required between adjacent electrodes to maintain electrical isolation and ensure a smooth transition of the phase profile introduced by the liquid crystal. Over the patterned ITO, a 200 nm-thick electrically insulating layer of SiO_2 is sputtered and into which small via openings (3μm×3μm) were etched, allowing electrical contact to be made to the underlying electrodes. An electrically conductive layer of Al is subsequently sputtered over the insulating layer to fill the vias and contact the electrodes and patterned to form eight independent electrical bus bars (6 μm wide within the lens).
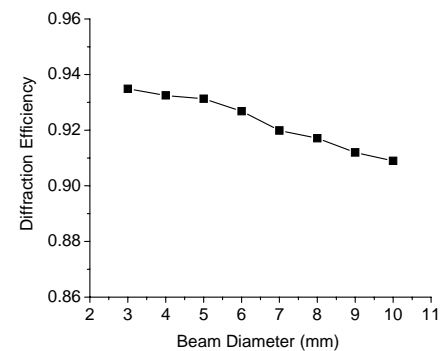

Fig. 9 Diffraction efficiency of the lens as a function of the beam diameter.

The patterned substrate, as well as an additional substrate with a continuous ITO electrode that acts as the electrical ground, were spin coated with poly (vinyl alcohol) to act as liquid crystal alignment layer. The alignment layers were rubbed with a velvet cloth to achieve homogeneous alignment and the two substrates were assembled. The commercial nematic liquid crystal E7 (Merck) was used as the electro-optic medium and was filled by capillary action into the empty cell at a temperature above the clearing point (60°C) and then cooled at 1°C/minute to room temperature. The cell was then sealed with epoxy and connected to the drive electronics. The drive electronics con-

sist of custom fabricated integrated circuits that contain eight independently controlled output channels. Each channel generates a modified square waveform with variable peak-to-peak amplitude between 0 and 5 V.

The lens showed excellent performance. In the optically inactive state (voltage off) in which the lens has no focusing power, optical transmission is 85% over the visible spectrum, a value that can be increased by the use of ophthalmic quality substrates and anti-reflection coatings. Eight optimized drive voltages with amplitudes between 0 and $2V_{rms}$ produced a maximum first-order diffraction efficiency of 91%, near the 95% predicted by scalar diffraction theory. The measured diffraction efficiency as a function of lens area reaches 94% near the center of the lens, decreasing monotonically as the area is increased (Fig. 9). The decrease is due to the fact that phase distortion caused by the fringing field at the zone boundaries has more significant effect at the outer zones as the width of each electrode becomes smaller. At the edges of the electrodes the electric field lines are not perpendicular to the liquid crystal lens substrate and the fringing fields cause the phase transitions at the zone boundaries to be not as sharp as in the ideal case; thus inducing phase distortions and reducing the diffraction efficiencies. The focused spot size is about 135 μm, which is also close to the diffraction-limit value of 133 μm. The lens shows sub-second switching time.
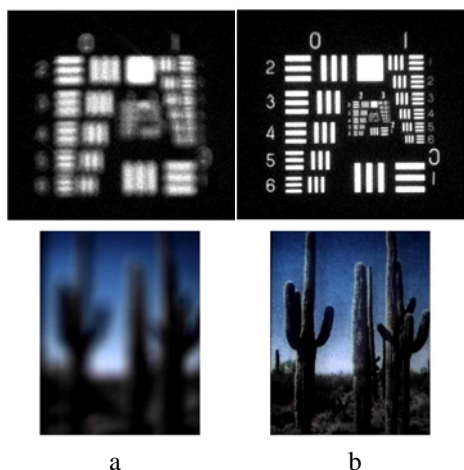

<div align="center">a　　　　　　　　b</div>

Fig. 10 Hybrid imaging using the 1-diopter electro-active diffractive lens with the model eye. The function of the diffractive lens is to provide near vision correction to the model eye. (a) The object is placed at a reading distance (~30 cm). The image is severely out of focus in the model eye when the diffractive lens is OFF. (b) When the diffractive lens is activated, the object is imaged clearly.

To test the imaging properties of the lens a model human eye was constructed using a fixed, +60 diopter achromatic doublet glass lens and a monochrome CCD with a filter to match the human photopic response. As homogeneously aligned nematic liquid crystals are polarization sensitive, two lenses with orthogonal alignment directions were used in series to create a single polarization insensitive lens. Two such lenses were aligned and cemented together. To simulate a typical near vision task such as reading, a double element lens was placed in front of the model eye and used to image a test object illuminated with unpolarized white light placed 30 cm in front of

the lens. As can be seen in Fig. 10a, the model eye has insufficient power to form a sharp image but by switching on the diffractive lens the image is brought into focus (Fig. 10b). The double element lens has excellent optical transmission. To test the imaging performance of the lenses with actual human subjects a pair of test spectacles has been constructed (Fig. 11) and initial clinical results agree well with the model eye test. When the electro-optic lenses are both in the inactive state, there is no noticeable degradation in the quality of the distant vision. For chromatic aberration, an achromatic diffractive lens can be designed by introducing p2π (p>1, integer) phase jump at the zone boundaries for the design wavelength. In practice, the ocular lens itself has a chromatic aberration which is less than the diffractive lens. Assuming the brain is adapted to a certain degree of chromatic aberration, balancing the dispersion of the diffractive lens and the eye is less desirable. More clinical study will be performed on this.
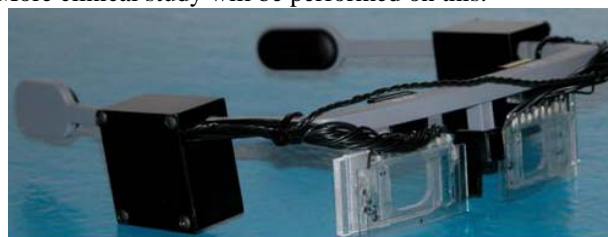

Fig. 11 A prototype of the assembled adaptive eyewear.

REFERENCES

[1] J T. Qiu, L. Li, A. Schülzgen, V. L. Temyanko, T. Luo, S. Jiang, A. Mafi, J. V. Moloney, and N. Peyghambarian, "Generation of 9.3-W multimode and 4-W single-mode output from 7-cm short fiber lasers," IEEE Photon. Technol. Lett. 16, p. 2592, 2004.

[2] P. Russell, *Photonic crystal fibers,* Science 299, p. 358, 2003.

[3] L. Li, A. Schülzgen, V. L. Temyanko, S. Sabet, M. M. Morrell, H. Li, A. Mafi, J. V. Moloney, and N. Peyghambarian, "Investigation of Modal Properties of Microstructured Optical Fibers with Large Depressed-Index Cores," Opt. Lett. 30, p. 3275, 2005.

[4] B. Hitz, "Fiber Laser Generates 1.6 W in Single Longitudinal Mode", Photon. Spectra 12, p. 110, 2005.

[5] N. Peyghambarian, T. Qiu, P. Polynkin, A. Schülzgen, L. Li, V. L. Temyanko, M. Mansuripur, and J. V. Moloney, "Short Fiber Lasers Produce Record Power/Length of 1.33W/cm," Opt. & Photon. News 15 (12), 41 (2004), Opt. in 2004.

[6] N. Peyghambarian and Axel Schülzgen, "Fiber Lasers, High Power Devices in Compact Packages," Opt. and Photon. News 16 (6), 36 (2005).

[7] S. Suzuki, A. Schülzgen, S. Sabet, J. V. Moloney, and N. Peyghambarian, "Photosensitivity of Ge-Doped Phosphate Glass to 244 nm Irradiation," Appl. Phys. Lett. 89, 171913 (2006).

[8] J. Albert, A. Schülzgen, V. L. Temyanko, S. Honkanen, and N. Peyghambarian, "Strong Bragg gratings in Phosphate Glass Single Mode Fiber," Appl. Phys. Lett. 89, 101127 (2006).

[9] L. Li, A. Schülzgen, V. L. Temyanko, M. M. Morrell, S. Sabet, H. Li, J. V. Moloney, and N. Peyghambarian, "Ultra-Compact Cladding-Pumped 35-mm-Short Fiber Laser with 4.7-W Single- Mode Output Power," Appl. Pys. Lett. 88, 161106 (2006).

[10] A. Schülzgen, L. Li, V. L. Temyanko, S. Suzuki, J. V. Moloney, and N. Peyghambarian, "Single-Frequency Fiber Oscillator with Watt-Level Output Power Using Photonic Crystal Phosphate Glass Fiber," Opt. Express 14, 7087 (2006).

[11] L. Li, A. Schülzgen, S. Chen, V. L. Temyanko, J. V. Moloney, and N. Peyghambarian, "Phase Locking and In-Phase Supermode Selection in Monolithic Multicore Fiber Lasers," Opt. Lett. 31, 2577 (2006).

[12] S. Marder, B. Kippelen, A.K.-Y Jen, and N. Peyghambarian, "Recent advances in the design and synthesis of chromophores and polymers for electro-optic and photorefractive applications," Nature, 388, 845 (1997).

[13] N. Peyghambarian, L. Dalton, A. Jen, B, Kippelen, S. Marder, R. Norwood, and J. Perry, "Technological advances brighten horizons for organic nonlinear optics," Laser Focus World, 42, 85 (2006).

[14] N. Peyghambarian and R. A. Norwood, "Organic Optoelectronics Materials N. and Devices for Photonic Applications, Part One," Opt. and Photon. News, 16, 2, 30-35 (2005).

[15] N. Peyghambarian and R. A. Norwood, "Organic Optoelectronics Materials and Devices for Photonic Applications, Part Two," Opt. & Photon. News, 16, 4, 28-33 (2005).

[16] K. Meerholz, B. L. Volodin, Sandalphon, B. Kippelen, and N. Peyghambarian, "A photorefractive polymer with high optical gain and diffraction efficiency near100%," Nature, 371, 497 (1994).

[17] B. L. Volodin, B. Kippelen, K. Meerholz, N. Peyghambarian, and B. Javidi, "A polymeric optical pattern-recognition system for security verification," Nature 383, 58 (1996).

[18] S. Tay, J. Thomas, M. Eralp, G. Li, B. Kippelen, S. R. Marder, G. Meredith, A. Schülzgen, and N. Peyghambarian, "Photorefractive polymer composite operating at the optical communication wavelength of 1550 nm," Appl. Phys. Lett., 85, 4561 (2004).

[19] M. Eralp, J. Thomas, S. Tay, G. Li, G. Meredith, A. Schülzgen, and N. Peyghambarian, "High-performance photorefractive polymer operating at 975nm wavelength," Appl. Phys. Lett., 85, 1095 (2004).

[20] S. Tay, J. Thomas, M., Eralp, G. Li, R. A. Norwood, A. Schülzgen, M. Yamamoto, S. Barlow, G. A. Walker, S. R. Marder, and N. Peyghambarian, "High performance photorefractive polymer operating at 1550 nm with near video-rate response time," Appl. Phys. Lett., 87, 171105 (2005).

[21] J. Thomas, M. Eralp, S. Tay, G. Li, M. Yamamoto, R. A. Norwood, S. R. Marder, and N. Peyghambarian, "Photorefractive polymers with superior performance," Opt. and Photon. News, 16, 31 (2005).

[22] M. Eralp, J. Thomas, S. Tay, G. Li, A. Schülzgen, R. A. Norwood, M. Yamamoto, and N. Peyghambarian, "Photorefractive polymer device with video-rate response time operating at low voltages," Opt. Lett., 31, 10, 1408-1410 (2006)

[23] B. Kippelen, S. R. Marder, E. Hendrickx, J. L. Maldonado, G. Guillemet, B. L. Volodin, Y. Enami, Sandalphon, Y. J. Yao, J. F. Wang, H. L. Erskine, and N. Peyghambarian, "Infrared photorefractive polymers and their applications for imaging," Science, 279, 54 (1998).

[24] M. Eralp, J. Thomas, S. Tay, G. Li, A. Schülzgen, R. A. Norwood, M. Yamamoto, M. and N. Peyghambarian, "Sub-millisecond response of a photorefractive polymer under single nanosec-

ond pulse exposure," Appl. Phys. Lett., 89, 114105 (2006).

[25] Y. Enami, G. Meredith, and N. Peyghambarian, "Hybrid electro-optic polymer/sol-gel waveguide modulator fabricated by all-wet etching process," Appl. Phys. Lett., 83, 4692 (2003).

[26] Y. Enami, G. Meredith, M. Kawazu, A. K-Y. Jen, and N. Peyghambarian, "Hybrid electro-optic polymer and selectively buried sol-gel waveguides," Appl. Phys. Lett., 82, 490 (2003).

[27] Y. Enami, C. T. DeRose, C. Loychik, D. Mathine, R. A. D. Norwood, J. Luo, J., A.K-Y Jen, and N. Peyghambarian, "Low half-wave voltage and high electro-optic effect in hybrid polymer/sol-gel waveguide modulators," Appl. Phys. Lett., 89, 143506 (2006).

[28] C.T. DeRose, Y. Enami, C. Loychik, R. A. Norwood, D. Mathine, M. Fallahi, N. Peyghambarian, J. D. Luo, A. K.-Y. Jen, M. Kathaperumal, and M. Yamamoto, "Pockel's coefficient enhancement of poled electro-optic polymers with a hybrid organic-inorganic sol-gel cladding layer," Appl. Phys. Lett., 89, 131102 (2006).

[29] H. Gan, H. Zhang, C. T. DeRose, R. Norwood, M. Fallahi, J. Luo, A.K.-Y. Jen, B. Liu, S. T. Ho, and N. Peyghambarian, "A hybrid Fabry-Pérot étalon using an electro-optic polymer for optical modulation," Appl. Phys. Lett., 89, 141113 (2006).

[30] H. Gan, H. Zhang, C. T. DeRose, R. Norwood, N. Peyghambarian, J. Luo,B. Chen, B., A. K.-Y. Jen, and M. Fallahi, "Low drive voltage Fabry-Perot etalon device tunable filters using poled hybrid sol-gel materials," Appl. Phys. Lett., 89, 041127 (2006).

[31] G. Li, D. L. Mathine, P. Valley, P. Äyräs, J. N. Haddock, G. Malahalli, G. Williby, J. Schwiegerling, G. R. Meredith, B. Kippelen, S. Honkannen, and N. Peyghambarian, "Switchable electro-optic diffractive lens with high efficiency for ophthalmic applications," Proceedings of the National Academy of Sciences, 103, 6100 (2006).

[32] G. Li, P. Valley, M. S. Giridhar, D. L. Mathine, G. Meredith, J. N. Haddock, B. Kippelen, and N. Peyghambarian, "Large-aperture switchable thin diffractive lens with interleaved electrode patterns," Appl. Phys. Lett., 89, 141120 (2006).

[33] N. Peyghambarian, G. Li, D. Mathine, P. Valley, J. Schwiegerling, S. Honkanen, P. Ayras, J. N. Haddock, G. Malalahalli, and B. Kippelen, "Electro-optic adaptive lens as a new eyewear,"

Molecular Crystals & Liquid Crystals, 454, 157 (2006).

[34] G. Li, D. Mathine, P. Valley, P. Aryas, J. Haddock, M. Giridhar, J. Schwiegerling, G. Meredith, N. Kippelen, S. Honkanen, and N. Peyghambarian, "Switchable diffractive lens for vision correction," Opt. and Photon. News, 17, No. 12, P. 28 (2006).